Earth Planets Space, **61**, 505–512, 2009

Upward propagating tidal effects across the *E*- and *F*-regions of the ionosphere

Thomas J. Immel[1], Scott L. England[1], Xiaoli Zhang[2], Jeffrey M. Forbes[2], and Robert DeMajistre[3]

[1]*Space Sciences Laboratory, University of California, Berkeley*
[2]*Department of Aerospace Engineering, University of Colorado, Boulder*
[3]*Applied Physics Laboratory, Johns Hopkins University, Laurel, Maryland*

(Received October 22, 2007; Revised April 7, 2008; Accepted May 14, 2008; Online published May 14, 2009)

Recent far-ultraviolet (FUV) observations of Earth have shown the remarkable spatial correspondence between the amplitude of non-migrating atmospheric tides originating in the troposphere and the density and morphology of the nighttime equatorial ionospheric anomaly (EIA). This is likely a result of the modulation of the *E*-region dynamo electric field in daytime by the tidal winds. FUV observations around the time of the vernal equinox of 2002 show that the signature of tidal influence, the wave-4 periodicity in the separation and density of the two EIA bands, itself exhibits significant temporal variability. Here, we seek to understand this variability, and whether (or not) it is linked to variations in the strength of the upward-propagating tides. This study relies on tidal measurements provided by the global observations from the TIMED-SABER instrument that measures the temperature variations in the MLT associated with the upward-propagating tides. TIMED-GUVI provides *F*-region density measurements concurrent to the MLT temperature retrievals. It is found that the atmospheric and ionospheric zonal wave-4 signatures very nearly covary over a 30-day period, strongly supporting the theory that the influence of the the diurnal eastward 3 (DE3) tide originating in the troposphere extends to the *F*-layer of the ionosphere. Additionally, a 6-day periodicity in the power of the ionospheric wave-4 signature is found that may originate with the tide's interaction with longer period planetary waves.

Key words: Atmospheric tides, tides and planetary waves, FUV, airglow, equatorial ionosphere, thermospheric dynamics.

1. Introduction

Earth's ionosphere is most dense at low latitudes where, in daytime, ionization rates of the neutral atmosphere reach a peak in the vicinity of the subsolar point. Solar extreme ultraviolet (EUV) radiation drives the processes that produce molecular and atomic ions, the former of which dominate the *E*-region (110–180 km), while the latter make up the main density peak of the ionosphere, the *F*-layer. The neutral atmosphere at ionospheric altitudes is heated by the same EUV forcing and thereby put into motion, flowing across pressure gradients centered on the dayside. The circulation of neutral gas has zonal and meridional components that drag plasma across Earth's magnetic field, and combine to generate dynamo electric fields and currents that further redistribute plasma (cf. Heelis, 2004). The resultant daytime electric fields at low latitudes are eastward, and in the vicinity of the dip equator their effect is to cause the plasma to convect upward and poleward, to altitudes where recombination is less rapid. This, combined with the gravitational potential of the uplifted plasma and its tendency to diffuse along the magnetic field, serves to produce peaks in density to either side of the dip equator. This structure is often referred to as the equatorial ionospheric anomaly (EIA) and the process that forms these peaks is the so-called "fountain effect".

In the *E*-region, ion densities drop drastically at night, greatly reducing the interaction between neutral winds and plasma in the lower ionosphere/thermosphere in favor of the continued dynamo effects occurring at higher altitudes. Upper-atmospheric neutral winds do effect changes in the density profile and height of the *F*-layer (cf. Colerico *et al.*, 1996), but the large-scale nighttime morphology is not greatly affected except during large magnetic storms, and then mainly by storm-time electric fields (Fejer, 1997; Richmond *et al.*, 2003; Immel *et al.*, 2005). Continuous FUV observations of the nightside ionosphere provided by experiments such as those onboard NASA's IMAGE and TIMED mission therefore provide a time-history of the daytime processes, hours after those processes have ceased to add to or modify the plasma. The major change in the *F*-layer of the ionosphere at night is the fairly rapid reduction in its density. The FUV emissions measured at 135.6 nm originate in the recombination of ionospheric O^+ and therefore decrease in intensity as the plasma co-rotates with Earth and drifts across the nightside. The underlying morphology is not significantly affected by this reduction in density with time (cf. England *et al.*, this issue). The sensitivity of the TIMED FUV instrument allows it to provide useful measurements from the evening terminator to beyond midnight, as is demonstrated in this report.

The daytime processes that drive the development of the ionosphere vary slowly with solar cycle and season (Fejer *et al.*, 1979). Shorter term variability of the ionosphere (2–30 days) has been observed from ground stations that can be

attributed to a number of sources including solar wind conditions, planetary atmospheric waves, and F-region neutral winds (Forbes *et al.*, 2000). Variability in the daytime electric fields on time scales shorter than one day can produce longitudinal variation in the growth of the F-layer. Variability on these times scales is often attributed to atmospheric tides. Effects of atmospheric tides on the ionosphere has long been studied experimentally with conclusive results regarding diurnal lunar and solar tides (Evans, 1978) and planetary wave effects (Canziani *et al.*, 1990; Pancheva *et al.*, 2006). Early modeling studies showed the importance of tidal coupling to the development of the ionosphere (Bernhardt *et al.*, 1976; Forbes and Lindzen, 1976; Volland, 1976).

A new set of observations have brought new light to the importance of the tides to the development of the ionosphere, and a significant longitudinal structure that they may introduce. Using global-scale FUV images from the NASA IMAGE satellite, Sagawa *et al.* (2005) identified the zonal wavenumber-4 ($s = 4$) zonal periodicity in the density and separation of the two bands of the equatorial ionospheric anomaly and suggested the likely importance of zonally dependent tidal forcing. Immel *et al.* (2006) noted that the covariation of these parameters ruled out nightside processes as forcing mechanisms, and favored the modulation of daytime E-region dynamo electric fields by diurnal forcing of an eastward propagating wavenumber-3 tide. These two observations depended upon the then-recent incorporation of tropospheric forcing effects into the Global Scale Wave Model (GSWM) by Hagan and Forbes (2002, 2003), including heating terms originating in both deep tropical convection and the absorption of solar infrared radiation by water vapor. Both England *et al.* (2006a) and Immel *et al.* (2006) made comparisons to FUV observations from TIMED-GUVI, while England *et al.* noted the wave-4 signature in EIA brightness was observed in OGO-4 630.0-nm data in October of 1967, though not discussed then or since Thuillier *et al.* (2002). England *et al.* (2007) demonstrated using the SAMI2 ionospheric model (Huba *et al.*, 2000) that a modest 40% modification of the daytime electric field can introduce changes in the EIA morphology consistent with the FUV observations. Furthermore, England *et al.* (2006b) used daytime passes from space-borne magnetometers to demonstrate that the longitudinal variation in the equatorial electrojet (reported earlier by Jadhav *et al.* (2002) and others) corresponds well to both the observed variation in the EIA and the tidal wind variations above 100 km from the GSWM. Recently Lin *et al.* (2007) and Kil *et al.* (2007) have noted the wave-4 pattern in GPS occultations and in-situ density data. Hagan *et al.* (2007) worked the lower-atmospheric tides into the lower boundary of the first-principles TIMEGCM model for simulations of the 2002 equinox period and found that the tidal forcing at around 30 km propagated upward and provided coherent forcing of winds in the lower ionosphere, modifying the E-region neutral wind dynamo and thereby enforcing longitudinally-dependent changes on the uplift of plasma. This resulted in a longitudinally-dependent development of the EIA with for major peaks, corresponding well to the early results from IMAGE (Immel *et al.*, 2006). This was the first model to provide the needed confirmation of the connection of tides originating in the troposphere to conditions in the ionospheric F-layer.

To confirm the connection experimentally, one must simultaneously obtain information pertaining to both the tidal winds in the E-region and the ionospheric conditions in the F-region. This unique combination of observations is provided by the NASA TIMED satellite. During nighttime passes, the Global Ultraviolet Imager (GUVI, Christensen *et al.* (2003)) measures ultraviolet emissions of the F-region ionosphere from nadir to limb along the TIMED orbit track, while the Sounding of the Atmosphere using Broadband Emission Radiometry experiment (SABER, Russell *et al.* (1999)) retrieves temperatures at the limb from 20 to 120 km altitude. Deviations in the mesospheric/lower-thermospheric (MLT) temperatures from a zonal mean can indicate horizontal convergence and divergence of neutral winds at these altitudes, a manifestation of tidal forcing. Measurements of the temperatures from the equator to high latitudes in every orbit allow for retrieval of the average phase and amplitude of particular tidal components over the two month TIMED precession cycle. On shorter timescales, deviations from mean temperatures as a function of geographic location are still observed, but the particular tidal components responsible for the variations cannot be uniquely identified.

2. Atmospheric Tides, TIMED SABER and GUVI Measurements

Atmospheric tides are driven by thermal forcing and, as such, consist of a significant diurnal, westward migrating (sun-synchronous) component produced by solar radiational heating of the atmosphere through a variety of mechanisms that depend on altitude. Multiple tidal components exist, however, that propagate in a manner other than westward once per day. These originate in processes that either (1) are asymmetricly distributed around Earth, (2) provide a peak forcing function offset in time from the main solar heating, or (3) develop in nonlinear interactions between the main migrating components and other planetary-scale atmospheric wave modes (cf. Forbes and Wu, 2006). These can have a higher wavenumber than the diurnal migrating component ($s = 1$ for the diurnal tide), and also significant components with 12- or 8-hour periods. From a single orbiting platform, it is impossible to draw out all the tidal components for a given day, or even in the long term without the possibility of aliasing of other lower and higher order components and long-term trends into the component of interest. There are several approaches that yield information on atmospheric tides from satellite data, each with their particular shortcomings and advantages (recently summarized by Zhang *et al.* (2006)). However, the effects of the tides on winds and temperatures in the MLT region are often large, with $\pm 50^{\circ}$K zonal variations with a distinct wave-like signature. Some attribution of these effects to particular candidate tidal components can therefore be made by surveying the daily temperature data, and this approach is taken here.

The time period of interest here is March–April, 2002, when the afore mentioned zonal variation in the characteristics of the EIA were observed by both IMAGE-FUV and

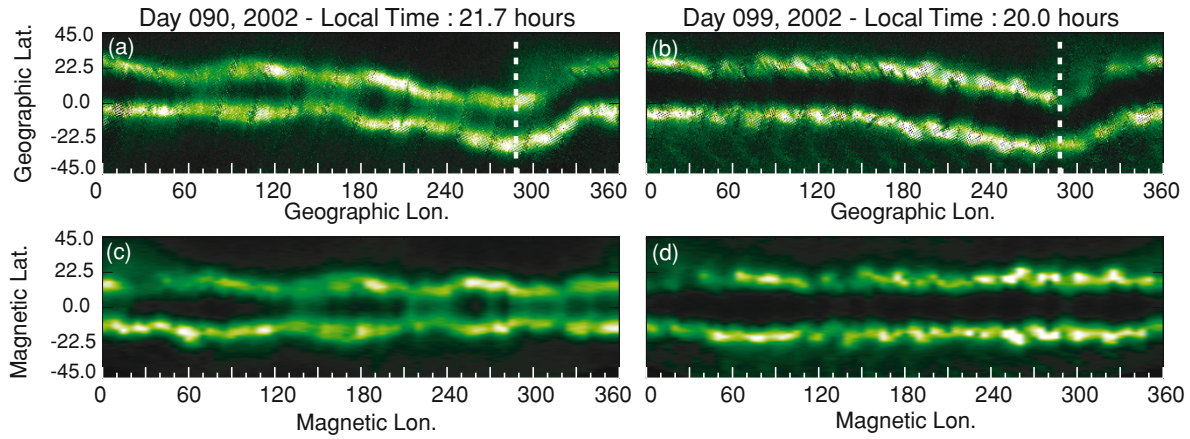

Fig. 1. 3-day averages of GUVI 135.6-nm disk observations, centered on days 90 and 99. 1a,b) Days 90 and 99 in original geographic coordinates. Geomagnetic longitude = 0° is indicated by a white dashed line. Figure 1(c, d) shows the same data rebinned into magnetic coordinates, with latitudinal and longitudinal resolution of 1° × 5°.

TIMED-GUVI (Sagawa *et al.*, 2005; Immel *et al.*, 2006). Earlier studies of this time period excluded FUV observations when the K_p index indicated moderate magnetic activity. For instance England *et al.* (2006a) required that the 3-hour K_p index be below 4 during any period of observations. In order to produce contiguous dataset for this study, observations during all levels of magnetic activity are included, where between days 70 and 100 the daily mean of K_p was below 3^+ except on day 87. TIMED was fully operational after its December 2001 launch and taking data of the very luminous nighttime ionosphere as observed just after solar maximum. Average global FUV brightness images (@135.6-nm) can be constructed from multiple orbits using 24 or more hours of data. For this work, 72-hour average brightness is calculated so as to provide continuous zonal coverage while only using irradiances obtained within 75° of nadir (TIMED is in a non-repeating orbit).

These can subsequently be mapped to APEX magnetic coordinates (Richmond, 1995) and the zonal variability characterized by the magnetic-latitudinal separation of the two peaks of the EIA. The separation serves as a proxy for the integrated daytime uplift of plasma that is here asserted to suffer a longitudinally-dependent tidal influence. This parameter is preferred to either the brightness or retrieved N_mF_2, as these latter two can be influenced by interhemispheric winds or the general wave-1 signature in EIA density that can appear due to the offset of the magnetic dipole from Earth's axis (Thuillier *et al.*, 2002). Two examples of daily FUV intensity maps and their magnetic re-mapping are shown in Fig. 1, where the average local times of the observations are 21.7 and 20.0 hours, respectively. The white vertical line in the geographic mappings (Fig. 1(a, b)) indicates 0° magnetic longitude, for reference to the magnetic maps below (Fig. 1(c, d)). The mean irradiances in the magnetic mappings are calculated on a 1° × 5° latitude-longitude grid.

In the GUVI EIA observations during the 72-hour period centered on Day 90 and remapped to magnetic coordinates (Fig. 1(c)), there are 4 minima in EIA separation, the first in the magnetic 30°–45° range, and then at 140°, 235° and 315°. The first minimum is in the Atlantic sector where the northern anomaly irradiance is often weak and extended well to the north. As such, this is the least well determined of the four minima, where those at greater longitudes are more clear. By day 99 (Fig. 1(d)), this pattern is completely different, with the EIA exhibiting a very regular separation at all longitudes. Though the local times differ by almost two hours, studies with IMAGE-FUV that simultaneously access the entire nightside during this same period give ample reason to expect EIA morphology variations observed at one local time to appear in neighboring sectors. The coherence of the EIA signature across local time sectors was held in support of the original assertion that the structure in the EIA originated during its development on the dayside.

The EIA separation distance is determined for all nighttime GUVI data obtained between days 72 and 106, proceeding from postmidnight to evening local times (0100 to 1915, respectively). The separation is shown as a stack plot for these days in Fig. 2 demonstrating the variability in the wave-4 signature as well as its overall peak in prominence during the middle of the period around day 90. This can be quantitatively shown by applying a Fourier transform to each day of separation data to determine (1) the total wave power in the separation data and (2) the relative power in each of the spectral components in the EIA separation signature, particularly the $s = 4$ (90° wavelength) component. These two parameters for the period are shown in Fig. 3. Evident in Fig. 3 is the peak in total wave power around day 90, with sharp minima around day 82 and day 98. The portion of the wave power in the $s = 4$ component varies greatly, beginning below 30% before day 80, then slowly ramping upwards to reach a peak of 70% on day 92, subsequently dropping back to a low of 30% before the end of the observations. The notable quasi-periodicity in the $s = 4$ power with a frequency of ~7 days will be remarked upon later in this report. The equally notable non-symmetry in the wave-4 signature, is due to multiple factors, including dipole offset (Hagan *et al.*, 2007) and possibly the presence of other tidal components (cf. England *et al.*, this issue).

If tides are indeed responsible for the structure observed in the EIA, then higher wavenumber components should be dominant on days like Day 90, while on Day 99, one

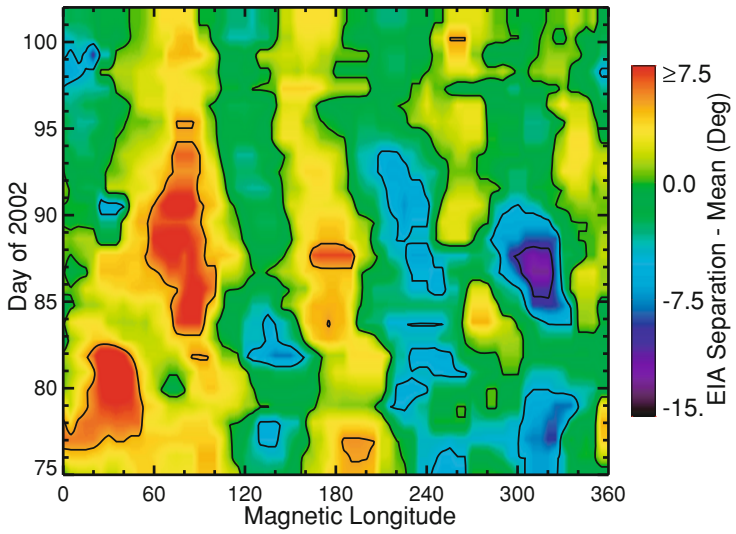

Fig. 2. Magnetic latitudinal separation of EIA bands at all magnetic longitudes as a function of day number. On each day, the mean daily separation is subtracted, showing departures from average. The generally 4-peaked signature is evident, as well as significant variability in this signature.

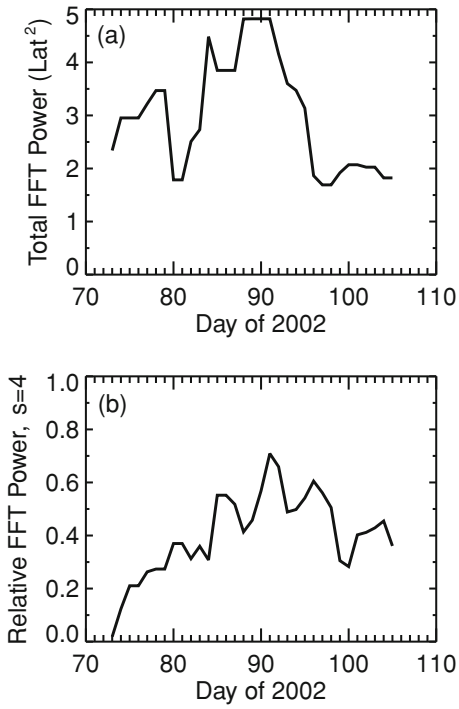

Fig. 3. Total and relative power in $s = 4$ component from Fourier analysis of EIA separation data shown in Fig. 2.

might expect much less power in high frequency tidal components, and/or an overall reduction in total tidal power. The validity of this hypothesis is investigated with TIMED SABER. Deviations from 60-day averaged zonal mean temperatures (at 110 km at the equator) as a function of geographic longitude and day of year are shown in Fig. 4. The period of nighttime imaging by GUVI is highlighted by the purple box. These residual temperature data are from the ascending node, mainly on the dayside as is evidenced in the right axis of the plot. A 4-peaked signature in temperature is present during this period, though it clearly changes in nature toward the end of the GUVI observation time. A similar treatment of the data by Forbes *et al.* (2006) for observations around autumnal equinox 2002 revealed a similar but more continuous wave-4 signature. Similar also to the earlier work, the data here are collected in a sliding five day window, that is shifted by four days at a time.

A spectral analysis of the temperature data can be performed using a Fourier transform in a manner similar to that applied to the GUVI EIA separation data (demonstrated in Fig. 3) with some differences. First, the temperature data are retrieved at nearly all latitudes excluding the polar regions. Only a subset of these measurements will have significance for the development of the EIA. For this first analysis, the daily mean of the temperature residuals in the $\pm 20^\circ$ geographic latitude range is determined. Secondly, temperature data are reported as a function of longitude in both the ascending and descending nodes of the orbit, while all the GUVI data in the day 72–106 period are from the ascending node. Observations in both nodes provide useful temperature measurements, though lacking complete knowledge of the amplitude and phase of the tidal components, the day and night measurements cannot be combined but must rather be treated separately. The results of the Fourier analysis for the descending and ascending nodes are shown in Fig. 5. Figures 5(a) and 5(b) show the total wave power reported by a fast-Fourier transformation of each five-day zonal temperature residual. The relative power in the $s = 4$ component (90 degree longitudinal wavelength) of these FFTs are shown in Figs. 5(c) and 5(d), respectively.

This analysis shows a remarkable variation in wave amplitudes in the descending node (daytime) with a 200% increase in wave power from day 70, reaching a peak on day 88 (Fig. 5(a)). Associated with the timing of this peak and every other daynumber reported in the SABER analysis is an uncertainty of two days, given the 4-day resolution of the averaged temperature residuals. On the nightside (Fig. 5(b)), there is an extended period of higher wave power between days 80 and 92 on the nightside. In each case, the power drops precipitously after the peak by factors of 3 and 2 on the dayside and nightside, respectively. For

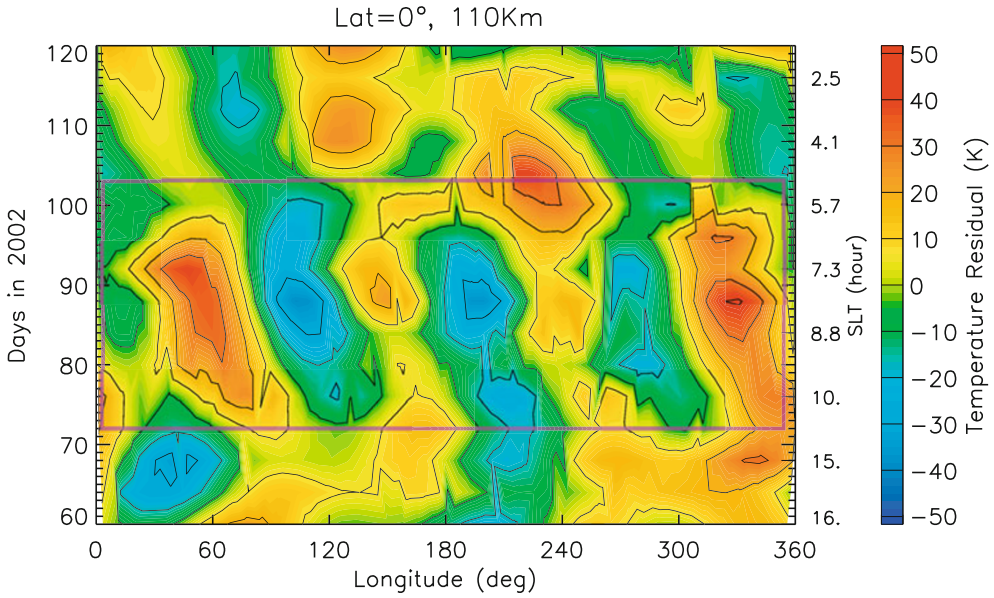

Fig. 4. Longitudinal distribution of temperature residuals at 100 km above the equator as a function of day of year for early 2002. These data are from descending node measurements, and the local time of observation is reported to the right. 4-day averages are interpolated to 1-day cadence.

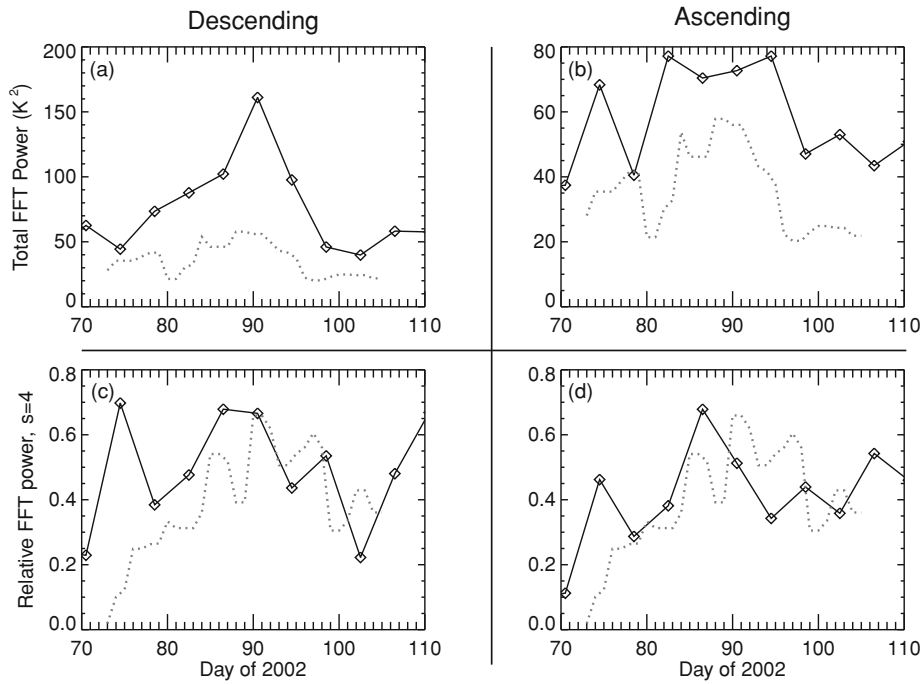

Fig. 5. Total and relative wave-4 power in the mean TIMED SABER temperature measurements in the ±20° latitude range. Total wave power reported by the Fourier analysis is shown descending (Fig. 5(a)) and ascending (Fig. 5(b)) nodes. The proportion of power in the $s = 4$ component of the Fourier transform is also shown for both descending (Fig. 5(c)) and ascending (Fig. 5(d)) nodes. Dashed lines show the Fourier components from the GUVI analyses (Fig. 3), where FFT power from Fig. 3(a) is shown, scaled arbitrarily but by the same factor in both Fig. 5(a) and 5(b).

comparison, the total wave power in the GUVI-measured EIA separation (from Fig. 3(a)) is shown with a dashed grey line (now in arbitrary units). It is evident that the wave power in the EIA morphology and SABER temperatures are similar, with peaks around day 90, and a precipitous drop in power before day 100 in all cases.

Examining the power in the $s = 4$ component of the Fourier analysis, on average during the period approximately 50% of the power in the FFT is in the $s = 4$ signature in both orbital nodes. Excursions above 60% in the day 80–90 range occur on both the dayside and nightside (Fig. 5(c), (d)), with minima occurring after day 90, particularly on the dayside with a minimum of 20% on day 100. These trends also bear similarity to the GUVI EIA separation $s = 4$ power, (from Fig. 3(b)) data that are overlaid (in their original units) on both plots. There appears to be a significant delay in the peak of $s = 4$ power in the EIA as compared to the SABER temperatures, though the EIA $s = 4$ minimum around day 100 appears well timed.

These observations lend clear support to the theory that

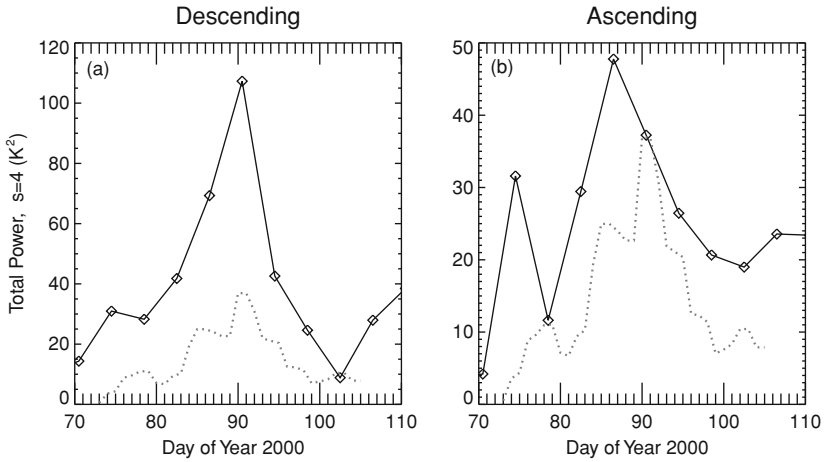

Fig. 6. Total wave-4 power in the mean TIMED SABER temperature measurements (solid line) and the GUVI EIA separation data (dashed line). The GUVI $s = 4$ power is in different units, and as such is scaled arbitrarily, but by the same factor in both Figs. 6(a) and 6(b).

the $s = 4$ structure is driven by atmospheric tides, in that a spectral analysis of the EIA and 110-km temperature data shows that both the total wave power and the relative power in the $s = 4$ component bear remarkable similarities. It is important to note that the actual power in the $s = 4$ temperature signature is the product of the total power and the relative $s = 4$ power (e.g. product of data in Fig. 5(a, c)). To complete the analysis, the $s = 4$ power is calculated for the temperature data from the ascending and descending nodes of the SABER as well as the GUVI EIA data and shown in Fig. 6. Here again, the same GUVI data are shown with a dashed grey line in each of the SABER plots, again in arbitrary but identical units in the two plots. Here, the comparison shows the remarkable similarity between the GUVI and SABER measured $s = 4$ signatures.

The 4-peaked signature in the tides is likely strongly related to the eastward propagating $n = 3$ diurnal tide, or DE3 in the widely adopted notation. In the fixed local time frame, the three peaks of this tide will propagate eastward by one wavelength once per day, resulting in the 4-peaked signature. Changes in tides such as the DE3 on short timescales can originate with changes in the nature of the source, (here, tropical cloud formation and water vapor), with modification of their amplitude and phase as they propagate through the stratosphere and mesosphere, or in non-linear interactions with large scale planetary waves at higher altitudes. Clearly, some combination of these factors is producing a modification in the tidal temperature signature with a 10-day timescale that is likely associated with variations in the DE3 tide. It is now known from several years of TIMED SABER observations that the signature of the DE3 tide above 100 km varies significantly in strength around vernal equinox (E. Talaat, private communications), varying from nearly nonexistent in mid-February to significantly strong in March–April, followed by another minimum in May. These observations indicate that a short-timescale minimum is also occurring in early April. Such a minimum would not necessarily be evident from the 60-day yaw-cycle temperature averages of TIMED SABER data necessary to fully characterize all tidal modes observable from that orbiting platform.

3. Discussion and Conclusion

The findings here show that, through the action of atmospheric tides, the troposphere exerts a controlling influence on the ionosphere at low latitudes. Short term variations in the global atmospheric tides, likely in this case an eastward propagating diurnal tide of wavenumber 3 (DE-3), produce similar short term variations in the ionosphere. This has been shown to most likely be related to interaction of the atmospheric tides and the ionosphere at E-region altitudes, generating electric fields that cause large-scale changes in the morphology of the F-layer. In that respect, the global morphology of the low latitude F-layer can serve as a good indicator of what tidal components are strong, and how the strength of those particular components varies with time. The prominence of individual tidal modes changes throughout the year, with concomitant effects in the EIA as noted in this issue by England *et al*. Recently Forbes *et al*. (2008) reported the remarkably large number of different tides observed the lower E-region of the ionosphere in the course of the first 5 years of the TIMED mission. Each of these may also have significant effects on ionospheric morphology.

Knowing that the EIA is quite sensitive to tidal forcing, it is interesting to revisit the results of the present analysis. The power in the zonal wave-4 signature in the EIA (cf. Fig. 3(b)) demonstrates a modulation on the order of 6 days, in striking similarity to the 6.5-day planetary wave (Talaat *et al*., 2001, 2002) that shows a peak in amplitude in the mesosphere and lower thermosphere during a period lasting 3–4 weeks around equinox. Though this may be a coincidence, it must be considered as a real effect, having now demonstrated the clear connection between tidal amplitudes in the E-region and F-region EIA morphology. An important question is then whether the signature of the 6-day wave is due to an in-situ enhancement to the neutral wind at the altitude of the E-layer, or rather a manifestation of the modification of the DE3 tide as it rises through the mesosphere. The height of the greatest zonal and meridional flow associated with the 6-day wave is therefore crucial to understanding this effect. Talaat *et al*. (2002) found that this altitude was just above 100 km, in general agreement with the modeling work of Meyer and Forbes (1997).

This is approximately 15–20 km lower than where the peak in the wind components from the upward propagating DE3 wave is found (Hagan and Forbes, 2002). Whether this separation is large enough to rule out direct forcing of the dynamo by the 6-day wave is a question that lies somewhat outside the scope of this work.

The 6-day periodic signature observed in the relative power of the $s = 4$ component of the EIA band separation is remarkably clear for what could be considered a secondary coupling effect, that is the possible modulation of upward propagating tidal energy by longer-period planetary waves in the mesosphere and lower thermosphere. The continuous ionospheric observations over a month in a slowly changing local time sector provide a wealth of data and, when treated properly, reveal effects that are difficult to discern from single ground stations. A larger survey is underway which may reveal more of these coupling effects and possible tidal components, the first results of which are reported by England *et al*. (this issue). The recent launches of 2 GUVI-type FUV imagers on DMSP satellites will likely yield another excellent long-term dataset.

Confirming the connection of atmospheric tides originating in the troposphere to ionospheric conditions has impacts that draw from other scientific fields. For instance, the El Niño-Southern Oscillation has been predicted to redistribute diurnal tidal energy out of non-migrating components (such as the DE3), and into the migrating component, due to the uniformity in heating inputs that the El Niño produces across the Pacific Ocean (Lieberman *et al*., 2007). This has immediate implications for the structure of the ionosphere, and implies the existence of an "ionospheric El Niño". With the continued development of new modeling techniques, expanded support for global-scale imaging, and new measurements of the important tidal winds and temperatures in the E-region, comes the possibility of significant new advances in aeronomy and in understanding of coupling processes throughout the atmosphere-ionosphere system.

Acknowledgments. This research is supported by NASA Heliophysics Guest Investigator Grant Numbers NNX07AG44G and NNG04GH05G. J. Forbes and X. Zhang acknowledge support under grants NNX07AB74G and NAG5-5028 from the NASA TIMED Program to the University of Colorado.

References

Bernhardt, P. A., D. A. Antoniadis, and A. V. da Rosa, Lunar perturbations in columnar electron content and their interpretation in terms of dynamo electrostatic fields, *J. Geophys. Res*., **81**, 5957–5963, 1976.

Canziani, P. O., A. E. Giraldez, and H. Teitelbaum, Thermospheric meridional wind tides above Argentina during 1984, *Ann. Geophys*., **8**, 549–557, 1990.

Christensen, A. B., *et al*., Initial observations with the Global Ultraviolet Imager (GUVI) in the NASA TIMED satellite mission, *J. Geophys. Res*., **108**, 1451, doi:10.1029/2003JA009918, 2003.

Colerico, M., *et al*., Coordinated measurements of F region dynamics related to the thermospheric midnight temperature maximum, *J. Geophys. Res*., **101**, 26,783–26,794, doi:10.1029/96JA02337, 1996.

England, S. L., T. J. Immel, E. Sagawa, S. B. Henderson, M. E. Hagan, S. B. Mende, H. U. Frey, C. M. Swenson, and L. J. Paxton, Effect of atmospheric tides on the morphology of the quiet time, post-sunset equatorial ionospheric anomaly, *J. Geophys. Res*., **111**, A10S19, doi:10.1029/2006JA011795, 2006a.

England, S. L., S. Maus, T. J. Immel, and S. B. Mende, Longitudinal variation of the E-region electric fields caused by atmospheric tides, *Geophys. Res. Lett*., **33**, L21105, doi:10.1029/2006GL027465, 2006b.

England, S. L., T. J. Immel, and J. D. Huba, Modeling the longitudinal variation in the post-sunset far-ultraviolet OI airglow using the SAMI2 model, *J. Geophys. Res*., **111**, A10S19, doi:10.1029/2006JA011795, 2007.

England, S. L., X. Zhang, T. J. Immel, J. M. Forbes, and R. DeMajistre, The effect of non-migrating tides on the morphology of the equatorial ionospheric anomaly: seasonal variability, *Earth Planets Space*, **61**, this issue, 493–503, 2009.

Evans, J. V., A note on lunar tides in the ionosphere, *J. Geophys. Res*., **83**, 1647–1652, 1978.

Fejer, B. F., D. T. Farley, R. F. Woodman, and C. Calderon, Dependence of equatorial F region vertical drifts on season and solar cycle, *J. Geophys. Res*., **84**, 5792–5796, 1979.

Fejer, B. G., The electrodynamics of the low-latitude ionosphere: recent results and future challenges, *J. Atmos. Sol.-Terr. Phys*., **59**, 1465–1482, 1997.

Forbes, J. M. and R. S. Lindzen, Atmospheric solar tides and their electrodynamic effects. I—The global Sq current system. II—The equatorial electrojet, *J. Atmos. Terr. Phys*., **38**, 897–920, 1976.

Forbes, J. M. and D. Wu, Solar Tides as Revealed by Measurements of Mesosphere Temperature by the MLS Experiment on UARS, *J. Atmos. Sci*., **63**, 1776–1797, 2006.

Forbes, J. M., S. E. Palo, and X. Zhang, Variability of the ionosphere, *J. Geophys. Res*., **62**, 685–693, 2000.

Forbes, J. M., J. Russell, S. Miyahara, X. Zhang, S. Palo, M. Mlynczak, C. J. Mertens, and M. E. Hagan, Troposphere-thermosphere tidal coupling as measured by the SABER instrument on TIMED during July–September 2002, *J. Geophys. Res*., **111**, A10S06, doi:10.1029/2005JA011492, 2006.

Forbes, J. M., X. Zhang, S. Palo, J. Russell, C. J. Mertens, and M. Mlynczak, Tidal variability in the ionospheric dynamo region, *J. Geophys. Res*., **113**, A02310, doi:10.1029/2007JA012737, 2008.

Hagan, M. E. and J. M. Forbes, Migrating and nonmigrating diurnal tides in the middle and upper atmosphere excited by tropospheric latent heat release, *J. Geophys. Res. (Atmos.)*, **107**, 4754, doi:10.1029/2001JD001236, 2002.

Hagan, M. E. and J. M. Forbes, Migrating and nonmigrating semidiurnal tides in the upper atmosphere excited by tropospheric latent heat release, *J. Geophys. Res*., **108**, 1062, doi:10.1029/2002JA009466, 2003.

Hagan, M. E., A. Maute, R. G. Roble, A. D. Richmond, T. J. Immel, and S. L. England, The effects of deep tropical clouds on the earth's ionosphere as simulated with ncar time-gcm, *Geophys. Res. Lett*., **34**, L20109, doi:10.1029/2007GL030142, 2007.

Heelis, R. A., Electrodynamics in the low and middle latitude ionosphere: a tutorial, *J. Atmos. Terr. Phys*., **66**, 825–838, doi:10.1016/j.jastp.2004.01.034, 2004.

Huba, J. D., G. Joyce, and J. A. Fedder, Sami2 is Another Model of the Ionosphere (SAMI2): A new low-latitude ionosphere model, *J. Geophys. Res*., **105**, 23,035–23,053, 2000.

Immel, T. J., J. C. Foster, A. J. Coster, S. B. Mende, and H. U. Frey, Global storm time plasma redistribution imaged from the ground and space, *Geophys. Res. Lett*., **32**, L03107, doi:10.1029/2004GL021120, 2005.

Immel, T. J., E. Sagawa, S. L. England, S. B. Henderson, M. E. Hagan, S. B. Mende, H. U. Frey, C. M. Swenson, and L. J. Paxton, The control of equatorial ionospheric morphology by atmospheric tides, *Geophys. Res. Lett*., **33**, L15108, doi:10.1029/2006GL026161, 2006.

Jadhav, G., M. Rajaram, and R. Rajaram, A detailed study of equatorial electrojet phenomenon using Ørsted satellite observations, *J. Geophys. Res*., **107**, 1175, doi:10.1029/2001JA000183, 2002.

Kil, H., S.-J. Oh, M. C. Kelley, L. J. Paxton, S. L. England, E. Talaat, K.-W. Min, and S.-Y. Su, Longitudinal structure of the vertical $\mathbf{E} \times \mathbf{B}$ drift and ion density seen from ROCSAT-1, *Geophys. Res. Lett*., **34**, L14110, doi:10.1029/2007GL030018, 2007.

Lieberman, R. S., D. M. Riggin, D. A. Ortland, S. W. Nesbitt, and R. A. Vincent, Variability of mesospheric diurnal tides and tropospheric diurnal heating during 1997–1998, *J. Geophys. Res*., **112**, D20110, doi:10.1029/2007JD008578, 2007.

Lin, C. H., *et al*., Plausible effect of atmospheric tides on the equatorial ionosphere observed by the FORMOSAT-3/COSMIC: Three-dimensional electron density structures, *Geophys. Res. Lett*., **34**, L11112, doi:10.1029/2007GL029265, 2007.

Meyer, C. K. and J. M. Forbes, A 6.5-day westward propagating planetary wave: Origin and characteristics, *J. Geophys. Res*., **102**, 26,173–26,178, doi:10.1029/97JD01464, 1997.

Pancheva, D. V. *et al*., Two-day wave coupling of the low-latitude

atmosphere-ionosphere system, *J. Geophys. Res.*, **111**, A07313, doi:10.1029/2005JA011562, 2006.

Richmond, A. D., Ionospheric electrodynamics using magnetic apex coordinates, *J. Geomag. Geoelectr.*, **47**, 191–212, 1995.

Richmond, A. D., C. Peymirat, and R. G. Roble, Long-lasting disturbances in the equatorial ionospheric electric field simulated with a coupled magnetosphere-ionosphere-thermosphere model, *J. Geophys. Res.*, **108**, 1118, doi:10.1029/2002JA009758, 2003.

Russell, J. M., M. G. Mlynczak, L. L. Gordley, J. J. Tansock, and R. W. Esplin, Overview of the SABER experiment and preliminary calibration results, in *Proc. SPIE Vol. 3756, p. 277–288, Optical Spectroscopic Techniques and Instrumentation for Atmospheric and Space Research III*, edited by A. M. Larar, vol. 3756 of *Presented at the Society of Photo-Optical Instrumentation Engineers (SPIE) Conference*, 277–288, 1999.

Sagawa, E., T. J. Immel, H. U. Frey, and S. B. Mende, Longitudinal structure of the equatorial anomaly in the nighttime ionosphere observed by IMAGE/FUV, *J. Geophys. Res.*, **110**, A11302, 2005.

Talaat, E. R., J.-H. Yee, and X. Zhu, Observations of the 6.5-day wave in the mesosphere and lower thermosphere, *J. Geophys. Res.*, **106**, 20,715–20,724, doi:10.1029/2001JD900227, 2001.

Talaat, E. R., J.-H. Yee, and X. Zhu, The 6.5-day wave in the tropical stratosphere and mesosphere, *J. Geophys. Res. (Atmos.)*, **107**, 4133, doi:10.1029/2001JD000822, 2002.

Thuillier, G., R. H. Wiens, G. G. Shepherd, and R. G. Roble, Photochemistry and dynamics in thermospheric intertropical arcs measured by the WIND Imaging Interferometer on board UARS: A comparison with TIE-GCM simulations, *J. Atmos. Sol.-Terr. Phys.*, **64**, 405–415, 2002.

Volland, H., Coupling between the neutral tidal wind and the ionospheric dynamo current, *J. Geophys. Res.*, **81**, 1621–1628, 1976.

Zhang, X., J. M. Forbes, M. E. Hagan, J. M. Russell, S. E. Palo, C. J. Mertens, and M. G. Mlynczak, Monthly tidal temperatures 20–120 km from TIMED/SABER, *J. Geophys. Res.*, **111**, A10S08, doi:10.1029/2005JA011504, 2006.

T. J. Immel (e-mail: immel@ssl.berkeley.edu), S. L. England, X. Zhang, J. M. Forbes, and R. DeMajistre